RSC Advances

PAPER

View Article Online
View Journal | View Issue

Cite this: *RSC Adv.*, 2025, **15**, 38865

1-Ethyl-4-butyl-1,2,4-triazolium acetyl amino acid ionic liquids: preparation and characterization of physicochemical properties

Kunhao Liang,[ab] Jie Meng,[a] Jing Qiao,*[ab] Lanju Liang,*[a] Dawei Fang[b] and Haiyun Yao*[a]

In order to address certain performance limitations of imidazolium amino acid ionic liquids, three novel 1-ethyl-4-butyl-1,2,4-triazolium acetyl amino acid ionic liquids, namely [Taz(2,4)][Acgly], [Taz(2,4)][Acala], and [Taz(2,4)][Accys] were synthesized and characterized in this work. Firstly, based on experimentally determined refractive indices and previously reported data including density, surface tension, viscosity, and heat capacity, the polarization properties, surface properties, and volumetric properties were calculated. Special emphasis was placed on elucidating the influence of acetyl amino acid anion structure on the physicochemical properties of these ionic liquids. Subsequently, by integrating molar surface Gibbs energy with the Lorentz–Lorenz relation, we established a predictive equation for surface tension, which demonstrated excellent agreement with experimental values. Analysis using the polarity coefficient equation revealed that the polarity of the ionic liquids decreases with increasing anion side-chain length, corresponding to enhanced hydrophobicity. Finally, the Eyring viscosity equation and thermodynamic formulas were employed to derive a computational expression for viscous flow activation energy, yielding results consistent with those obtained from the Arrhenius equation. Current limited research on 1-ethyl-4-butyl-1,2,4-triazolium acetyl amino acid ionic liquids necessitates combined experimental and semi-empirical approaches to guide their functional design and industrial applications.

Received 27th August 2025
Accepted 7th October 2025

DOI: 10.1039/d5ra06386h

rsc.li/rsc-advances

1. Introduction

Ionic liquids (ILs), recognized as green and designer solvents, have garnered significant attention and application across various industries.[1–5] While imidazolium cations are prevalent in current ILs, their inherent drawback lies in the acidic C_2 proton of the imidazolium ring. This acidity facilitates decomposition under basic conditions *via* carbene formation, potentially inducing side reactions.[6] Substituting imidazolium with triazolium cations—either 1,2,3-triazolium or 1,2,4-triazolium—mitigates this instability.[7–10] Given the hazardous azides typically employed in synthesizing 1,2,3-triazole derivatives, 1,2,4-triazolium is frequently the more suitable cationic platform.[11]

Amino acids are often employed as biocompatible anions to impart specific functionality to ILs.[12–16] A key limitation of amino acid-based ILs, however, is their relatively low thermal decomposition temperature compared to ILs with conventional anions, hindering broader application. The corresponding acetylated amino acids offer enhanced thermal stability and higher molar heat capacity compared to their amino acid precursors.[17] Consequently, this study focuses on the development and characterization of novel, non-toxic ionic liquids comprising 1-ethyl-4-butyl-1,2,4-triazolium cations paired with acetyl amino acid anions. Investigation of their thermal properties aims to support practical utilization.[18]

Although our prior work has evaluated the feasibility of these novel ILs as sustainable heat-transfer fluids,[19–24] their characterization primarily focused on key properties for thermal applications, such as heat capacity, thermal conductivity, heat-storage density, thermal stability, and heat-transfer coefficients/areas in heat exchangers. Nevertheless, research on triazolium acetyl amino acid ILs, particularly their fundamental physicochemical properties, remains far from exhaustive, given the vast potential for novel structural designs and applications. Industry advancement necessitates such development, driving the demand for robust methods to characterize physico-chemical properties. Accurate prediction of IL behavior *via* semi-empirical methods critically depends on this data.

Building upon prior work with ILs,[24,25] the compounds [Taz(2,4)][Acgly], [Taz(2,4)][Acala], and [Taz(2,4)][Accys] were synthesized. Their refractive indices were experimentally determined. Utilizing these refractive indices alongside established literature data (density, surface tension, viscosity, heat capacity),[24] a range of thermophysical properties were

[a]*School of Opto-Electronic Engineering, Zaozhuang University, Zaozhuang, Shandong 277160, China. E-mail: 17824951070@163.com*

[b]*Institute of Rare and Scattered Elements, College of Chemistry, Liaoning University, Shenyang, Liaoning 110036, China*

computed. It is noteworthy that while numerous studies have examined the impact of varying methylene chain lengths on cations (*e.g.*, imidazolium) on IL properties, analogous effects on anions remain comparatively underexplored.[26–29] Therefore, this study not only addresses the fundamental research gap left by the previous application-oriented work and advances the quantitative understanding of the structure–property relationships in this class of ILs, but also complements the fundamental database of ILs by offering new analytical tools and design concepts.

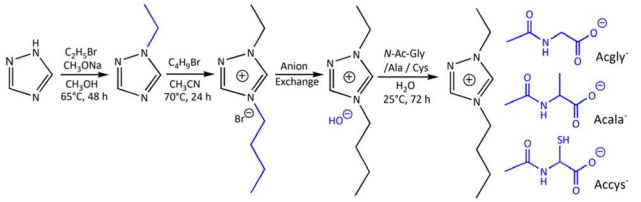

Fig. 1 Synthesis of the novel ILs [Taz(2,4)][Acgly], [Taz(2,4)][Acala] and [Taz(2,4)][Accys].

2. Experimental

2.1 Reagents

The CAS number, purities and sources of the reagents are listed in Table 1.

2.2 Preparation

In this study, the synthesis of ILs [Taz(2,4)][Acgly], [Taz(2,4)][Acala], andaz(2,4)][Accys] was accomplished through a four-step procedure, as illustrated in Fig. 1. Firstly, a mixture of 1,2,4-triazole, methanol, and sodium methoxide was reacted with bromoethane at 65 °C for 48 h to yield 1-ethyl-1,2,4-triazole. Secondly, the intermediate 1-ethyl-1,2,4-triazole was further reacted with bromopentane at 70 °C for 24 h to produce the bromide-based IL precursor, [Taz(2,4)][Br]. Then, [Taz(2,4)][Br] was dissolved in distilled water and passed through a pre-treated anion exchange column packed with Amberjet 4200-Cl resin. The effluent was collected once it showed strong alkalinity and the absence of bromide ions was confirmed by $AgNO_3$–HNO_3 testing, yielding [Taz(2,4)][OH]. Finally, the aqueous solution of [Taz(2,4)][OH] was reacted with an equimolar amount of *N*-acetyl-L-glycine/alanine/cysteine at room temperature to obtain the target ILs. The products were subsequently purified using organic solvents, including acetonitrile and dichloromethane.

2.3 Characterization

The [Taz(2,4)][Acgly], [Taz(2,4)][Acala] and [Taz(2,4)][Accys] were characterized by ^{1}H-NMR spectroscopy, ^{13}C-NMR spectroscopy, FT-IR spectroscopy and thermogravimetry (TG) (see Fig. S1–S12) and the water content was determined by a Karl Fischer moisture titrator (ZSD-2 type).

[Taz(2,4)][Acgly] was obtained as a light yellow transparent liquid. ^{1}H-NMR (DMSO-d_6): $\delta_H = 10.59$ (s, 1H), 9.32 (s, 1H), 7.55 (d, 1H), 4.44 (m, 2H), 4.26 (t, 2H), 3.43 (d, 2H), 1.84 (m, 5H), 1.49 (t, 3H), 1.32 (m, 2H), 0.93 (t, 3H). ^{13}C-NMR (DMSO-d_6): 172.03, 168.88, 144.91, 142.97, 47.22, 47.15, 43.34, 31.08, 22.71, 18.97, 13.79, 13.43. IR (500–4500 cm^{-1}, KBr pellet): 3294, 2964, 2935, 2883, 1954, 1457, 1364, 1164, 776. According to the whole TG curve, the sample initial decomposition temperature is about 453.16 K, and the mass fraction of water content is (0.00525 ± 0.0001). Thus, the purity of the [Taz(2,4)][Acgly] could be estimated more than 99%.

[Taz(2,4)][Acala] was obtained as a light yellow transparent liquid. ^{1}H-NMR (DMSO-d_6): $\delta_H = 10.61$ (s, 1H), 9.32 (s, 1H), 7.59 (d, 1H), 4.44 (m, 2H), 4.29 (t, 2H), 3.88 (m, 1H), 1.82 (m, 5H), 1.49 (t, 3H), 1.29 (m, 2H), 1.16 (d, 3H), 0.93 (t, 3H). ^{13}C-NMR (DMSO-d_6): 175.34, 168.05, 144.98, 143.15, 49.71, 47.21, 47.13, 31.12, 22.90, 19.04, 18.98, 13.80, 13.16. IR (500–4500 cm^{-1}, KBr pellet): 3400, 3274, 2966, 2930, 2877, 1651, 1594, 1454, 1398, 1164, 646. According to the whole TG curve, the sample initial decomposition temperature is about 453.67 K, and the mass fraction of water content is (0.00521 ± 0.0001). Thus, the purity of the [Taz(2,4)][Acala] could be estimated more than 99%.

[Taz(2,4)][Accys] was obtained as a colorless transparent liquid. ^{1}H-NMR (DMSO-d_6): $\delta_H = 10.59$ (s, 1H), 9.32 (s, 1H), 7.58 (d, 1H), 4.42 (m, 2H), 4.27 (t, 2H), 4.01 (m, 1H), 2.78 (m, 3H), 1.82 (m, 5H), 1.47 (t, 3H), 1.32 (m, 2H), 0.91 (t, 3H). ^{13}C-NMR (DMSO-d_6): 172.00, 168.87, 144.90, 142.98, 55.96, 47.25, 47.18,

Table 1 The CAS number, purity and source of the reagents

Reagent	CAS	Purity	Source
Bromoethane	74-96-4	99%	Shanghai Macklin Biochemical Co.,Ltd
Bromobutane	190-65-9	99%	Shanghai Macklin Biochemical Co.,Ltd
1,2,4-Triazole	288-88-0	99%	Shanghai Macklin Biochemical Co.,Ltd
N-Acetyl-glycine	543-24-8	99%	Shanghai Macklin Biochemical Co.,Ltd
N-Acetyl-L-alanine	97-69-8	99%	Shanghai Macklin Biochemical Co.,Ltd
N-Acetyl-L-cysteine	616-91-1	99%	Shanghai Macklin Biochemical Co.,Ltd
Methanol	67-56-1	99%	Tianjin Fuyu chemical Co.,Ltd
Sodium methoxide	124-41-4	99%	Shanghai Macklin Biochemical Co.,Ltd
Acetonitrile	75-05-8	99%	Tianjin Fuyu chemical Co.,Ltd
Dichloromethane	75-09-2	99%	Tianjin Fuyu chemical Co.,Ltd
Amberjet 4200-CL	60 177-39-1	Particle size > 0.950	Sinopharm Chemical Reagent Co., Ltd
Deionized water	—	—	Manufactured by multiple distillation

31.11, 27.14, 22.95, 19.01, 13.84, 13.47. IR (500–4500 cm^{-1}, KBr pellet): 3401, 3274, 2963, 2930, 2874, 1601, 1464, 1365, 1164, 776. According to the whole TG curve, the sample initial decomposition temperature is about 452.26 K, and the mass fraction of water content is (0.00344 ± 0.0001). Thus, the purity of the [Taz(2,4)][Accys] could be estimated more than 99%.

2.4. Determination of refractive indexes

The refractive index (n_D) was measured using a WZS-1 Abbe refractometer with an accuracy of ± 0.0002. The instrument was coupled with a GDH-2008W high-precision low-temperature thermostatic bath (ΔT = ± 0.02 K) to ensure temperature stability during measurements. Prior to measurement, the system was equilibrated at the target temperature for 30 minutes to achieve thermal stability. For hydrophilic ILs [Taz(2,4)][Acgly], [Taz(2,4)][Acala], and [Taz(2,4)][Accys] that readily form hydrogen bonds with water, the standard addition method (SAM) was employed to eliminate interference from residual water. Refractive index measurements were conducted across a temperature range of 288.15–323.15 K at 5 K intervals for ionic liquid samples with varying water contents. The intrinsic physical properties of anhydrous ILs were determined through linear regression analysis, where the intercept of the refractive index-water content curve provided the water-free reference value.

3. Results and discussion

3.1 Refractive index

The refractive index values of [Taz(2,4)][Acgly], [Taz(2,4)][Acala], and [Taz(2,4)][Accys] with varying water contents were determined as the average of triplicate measurements, summarized in Table 2 and represented in Fig. S13–S15. At constant temperature, the refractive index exhibited a linear correlation with water content (w_2), with all linear regression coefficients exceeding 0.99. Standard deviations of the regressions remained within experimental error ranges, confirming the validity of the SAM for these ILs. The intercepts of these linear

Table 2 Refractive index, n_D, values of [Taz(2,4)][Acgly], [Taz(2,4)][Acala] and [Taz(2,4)][Accys] containing various mass fraction of water, w_2, at T = (288.15–323.15) K[a]

T/K	$10^3\ w_2 = 5.25$	$10^3\ w_2 = 8.79$	$10^3\ w_2 = 11.76$	$10^3\ w_2 = 14.97$	$10^3\ w_2 = 17.68$	$10^3\ w_2 = 0$	r^2	sd $\times 10^{-5}$
[Taz(2,4)][Acgly]								
288.15	1.4953	1.4949	1.4945	1.4941	1.4937	1.4960	0.998	4.00
293.15	1.4941	1.4937	1.4933	1.4929	1.4926	1.4948	0.999	2.69
298.15	1.4929	1.4925	1.4921	1.4918	1.4915	1.4935	0.996	4.29
303.15	1.4920	1.4916	1.4912	1.4908	1.4905	1.4927	0.999	2.69
308.15	1.4911	1.4906	1.4902	1.4899	1.4895	1.4917	0.994	6.11
313.15	1.4899	1.4894	1.4891	1.4887	1.4883	1.4906	0.996	5.03
318.15	1.4886	1.4881	1.4878	1.4873	1.4870	1.4893	0.996	5.28
323.15	1.4873	1.4869	1.4865	1.4861	1.4857	1.4880	0.998	3.99
T/K	$10^3\ w_2 = 5.21$	$10^3\ w_2 = 8.46$	$10^3\ w_2 = 11.03$	$10^3\ w_2 = 13.28$	$10^3\ w_2 = 15.37$	$10^3\ w_2 = 0$	r^2	sd $\times\ 10^{-5}$
[Taz(2,4)][Acala]								
288.15	1.4920	1.4917	1.4914	1.4911	1.4909	1.4926	0.995	4.60
293.15	1.4911	1.4907	1.4904	1.4901	1.4899	1.4917	0.998	2.98
298.15	1.4901	1.4896	1.4893	1.4889	1.4887	1.4908	0.993	6.53
303.15	1.4890	1.4886	1.4882	1.4878	1.4876	1.4898	0.992	7.27
308.15	1.4878	1.4873	1.4869	1.4866	1.4863	1.4886	0.999	2.79
313.15	1.4860	1.4856	1.4851	1.4848	1.4845	1.4868	0.993	6.91
318.15	1.4844	1.4839	1.4836	1.4832	1.4829	1.4852	0.996	5.00
323.15	1.4826	1.4822	1.4818	1.4814	1.4811	1.4836	0.994	6.33
T/K	$10^3\ w_2 = 3.44$	$10^3\ w_2 = 7.45$	$10^3\ w_2 = 10.94$	$10^3\ w_2 = 14.07$	$10^3\ w_2 = 17.29$	$10^3\ w_2 = 0$	r^2	sd $\times\ 10^{-5}$
[Taz(2,4)][Accys]								
288.15	1.5183	1.5179	1.5175	1.5172	1.5168	1.5187	0.998	2.78
293.15	1.5172	1.5168	1.5164	1.5161	1.5158	1.5176	0.998	2.44
298.15	1.5162	1.5158	1.5154	1.5151	1.5148	1.5166	0.998	2.44
303.15	1.5149	1.5145	1.5141	1.5137	1.5134	1.5153	0.997	3.44
308.15	1.5134	1.5130	1.5126	1.5123	1.5120	1.5138	0.998	2.44
313.15	1.5113	1.5110	1.5107	1.5105	1.5102	1.5116	0.997	2.46
318.15	1.5101	1.5098	1.5096	1.5093	1.5091	1.5104	0.994	3.32
323.15	1.5089	1.5086	1.5084	1.5081	1.5079	1.5092	0.994	3.32

[a] Standard uncertainties u are $u(T)$ = 0.02 K, $u(p)$ = 0.01 MPa, $u(w_2)$ = 0.0001, and the expanded uncertainty $U(n_D)$ = 0.0032 with 0.95 level of confidence ($k \approx 2$); w_2 is the various mass fraction of water; r^2 is the correlation coefficient square and sd is the standard deviation.

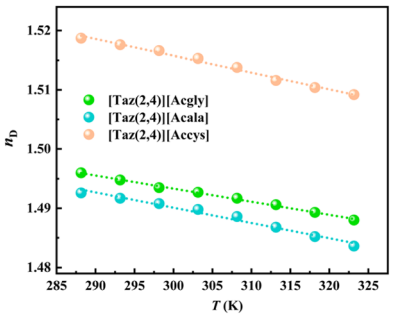

Fig. 2 Plot of refractive index, n_D, *versus* temperature, T. [Taz(2,4)][Acgly]: $n_D = 1.5599 - 2.2191 \times 10^{-4}\ T$, $r^2 = 0.99$, sd $= 5.21 \times 10^{-6}$; [Taz(2,4)][Acala]: $n_D = 1.5677 - 2.5881 \times 10^{-4}\ T$, $r^2 = 0.99$, sd $= 5.61 \times 10^{-6}$; [Taz(2,4)][Accys]: $n_D = 1.6008 - 2.8333 \times 10^{-4}\ T$, $r^2 = 0.99$, sd $= 6.77 \times 10^{-6}$.

fits provided the experimental refractive index values for anhydrous ILs (Fig. 2).

As shown in Table 2 and Fig. 2, the refractive index of anhydrous ionic liquids exhibits an inverse correlation with temperature, primarily attributed to thermal expansion-induced reduction in molecular packing density. Furthermore, introducing methylene groups or sulfur atoms into the IL anions reduced the refractive index. This observation aligns with prior studies: Almeida *et al.* reported that IL refractive indices depend on anion volume,[30] while Deetlefs *et al.* demonstrated that tighter packing of anions and cations correlates with higher refractive indices.[31] This phenomenon may arise from methylene/sulfur substitutions lowering refractive indices through increased anion volume and reduced polarizability.

State and liquid state in the corres

3.2 Derived properties

3.2.1 Polarization properties. According to the Lorentz–Lorentz relation for non-polar materials connecting the static refractive index with molecular polarizability,[32] the molar refraction (R_m) is defined as:

$$R_m = [(n_D^2 - 1)/(n_D^2 + 2)]V = (4\pi N/3)\alpha_P \quad (1)$$

where n_D is the refractive index and α_p represents the molar polarizability. The R_m and α_p values listed in Table 3 demonstrate that [Taz(2,4)][Acgly], [Taz(2,4)][Acala], and [Taz(2,4)][Accys] exhibit temperature-independent R_m and α_p, indicating that these parameters characterize the induced dipole effects in the ILs.

Table 3 Values of the refractive index (n_D), molar refraction (R_m), molar polarizability (α_p), and surface tension (γ) of [Taz(2,4)][Acgly], [Taz(2,4)][Acala] and [Taz(2,4)][Accys] in the range of $T = (288.15–323.15)$ K[a]

T/K	n_D	R_m/cm^3 mol^{-1}	$10^{24}\ \alpha_p$/cm^3	[a]γ/mJ m^{-2}	S_a/mJ K^{-1} m^{-2}	E_a/mJ m^{-2}
[Taz(2,4)][Acgly]						
288.15	1.4960	68.64	27.21	45.8	70.2	66.0
293.15	1.4948	68.69	27.23	45.5	70.2	66.1
298.15	1.4935	68.74	27.25	45.2	70.2	66.1
303.15	1.4927	68.85	27.29	44.9	70.2	66.2
308.15	1.4917	68.94	27.33	44.5	70.2	66.1
313.15	1.4906	69.00	27.35	44.1	70.2	66.1
318.15	1.4893	69.05	27.37	43.7	70.2	66.0
323.15	1.4880	69.10	27.39	43.4	70.2	66.1
[Taz(2,4)][Acala]						
288.15	1.4926	73.56	29.16	46.4	75.5	66.6
293.15	1.4917	73.68	29.21	46.1	75.5	66.7
298.15	1.4908	73.78	29.25	45.7	75.5	66.6
303.15	1.4898	73.88	29.29	45.3	75.5	66.6
308.15	1.4886	73.96	29.32	44.9	75.5	66.5
313.15	1.4868	73.96	29.32	44.5	75.5	66.5
318.15	1.4852	73.98	29.33	44.2	75.5	66.5
323.15	1.4836	74.01	29.34	43.8	75.5	66.5
[Taz(2,4)][Accys]						
288.15	1.5187	81.03	32.12	46.7	72.6	66.9
293.15	1.5176	81.12	32.16	46.4	72.6	67.0
298.15	1.5166	81.22	32.20	46.1	72.6	67.0
303.15	1.5153	81.29	32.23	45.7	72.6	67.0
308.15	1.5138	81.34	32.24	45.3	72.6	66.9
313.15	1.5116	81.28	32.22	44.9	72.6	66.9
318.15	1.5104	81.37	32.26	44.6	72.6	66.9
323.15	1.5092	81.45	32.29	44.2	72.6	66.9

[a] Derived from previous work.[24]

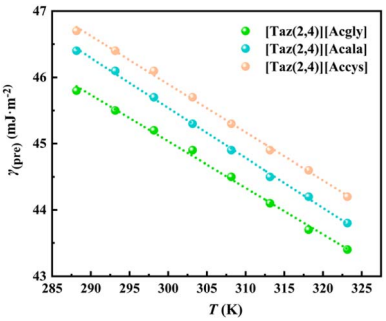

Fig. 3 Plot of surface tension, γ, *versus* temperature, T. [Taz(2,4)][Acgly]: $\gamma = 66.1–7.024 \times 10^{-2}\ T$, $r^2 = 0.996$, sd $= 1.72 \times 10^{-3}$; [Taz(2,4)][Acala]: $\gamma = 68.2–7.548 \times 10^{-2}\ T$, $r^2 = 0.999$, sd $= 1.07 \times 10^{-3}$; [Taz(2,4)][Accys]: $\gamma = 67.7–7.262 \times 10^{-2}\ T$, $r^2 = 0.998$, sd $= 1.35 \times 10^{-3}$.

3.2.2 Surface properties. The surface entropy (S_a) of a pure liquid, defined as the magnitude of the temperature-dependent slope of γ, quantifies the degree of surface disorder per unit volume. By applying a least-squares linear regression to the surface tension data of the ionic liquids (at zero water content) as a function of temperature (see Fig. 3), the empirical equation is derived:

$$\gamma = A_0 - S_a T \quad (2)$$

where A_0 is an empirical parameter and $S_a = -(\partial\gamma/\partial T)_p$ represents the surface entropy. The S_a values for [Taz(2,4)][Acgly], [Taz(2,4)][Acala], and [Taz(2,4)][Accys] are summarized in Table 3.

The surface energy (E_a) of ionic liquids can be calculated from their γ and S_a at zero water content using the equation:

$$E_a = \gamma - T(\partial\gamma/\partial T)_P \quad (3)$$

The calculated E_a values for the ILs at various temperatures are listed in Table 3. The results indicate that the surface energy of ionic liquids decreases with the elongation of alkyl chains on the anion or the introduction of sulfur atoms, which aligns with the observations reported by Yan and Wei.[23,33] This reduction is likely attributed to enhanced steric hindrance and diminished electronic effects within the ionic liquid structure. Furthermore, the E_a remains nearly constant across the temperature range of 288.15–323.15 K, indicating negligible temperature dependence of E_a. The temperature insensitivity of E_a can be attributed to the compensatory effect of S_a on energy variations and the dynamic equilibrium between intermolecular interactions and interfacial structures.[34,35]

Notably, the E_a of ILs is significantly lower than that of molten salts but closer to that of organic liquids. This suggests weaker interionic interactions in ILs compared to inorganic molten salts, as surface energy is determined by the strength of these interactions. The weaker interactions also explain the lower standard entropy of ILs relative to molten salts.[23]

3.2.3 Volumetric properties. The molecular volume (V_m) of an IL, defined as the combined volume of one cation and one anion, is calculated from density values using the equation:

$$V_m = M/(\rho N) = V/N \quad (4)$$

where M denotes molar mass, ρ represents density, N is Avogadro's constant, and V corresponds to molar volume. As shown in Table 3 for synthesized ILs at 298.15 K, the introduction of a methylene group (–CH_2–) or sulfur atom (–S–) into the anion significantly increases V_m, which is closely related to changes in steric hindrance and electron cloud distribution.[36]

Specifically, the volumetric contributions from a methylene group and sulfur atom in acetylated amino acid anions were quantified as $V_{m(-CH_2-)} = 0.0307$ nm^3 and $V_{m(-S-)} = 0.0229$ nm^3, respectively. The larger contribution from the methylene group likely stems from alkyl chain elongation, leading to linear molecular skeleton extension and cumulative van der Waals volume effects. In contrast, the relatively smaller contribution of sulfur atoms may be attributed to their enhanced electron polarizability. The higher electronegativity of sulfur promotes structural compactness in anions, partially offsetting steric effects.[37]

According to Glasser's theory,[19] the standard molar entropy (S^0) and the crystal energy (U_{POT}) of the ILs can be estimated:

Table 4 Volumetric contributions of a methylene group or a sulfur atom in anions at 298.15 K

ILs	M/g mol^{-1}	$^a\rho$/g cm^{-3}	$10^4\ V$/m^3 mol^{-1}	V_m/nm^3	$\Delta V_{m(-CH_2-)}$/nm^3	$\Delta V_{m(-S-)}$/nm^3
[Taz(2,4)][Acgly]	270.37	1.14395	2.363	0.3925	0.0307	
[Taz(2,4)][Acala]	284.41	1.11596	2.549	0.4232		0.0229
[Taz(2,4)][Accys]	316.48	1.17804	2.687	0.4461		

ILs	S^0/J K^{-1} mol^{-1}	$\Delta S^0_{(-CH_2-)}$/J K^{-1} mol^{-1}	$\Delta S^0_{(-S-)}$/J K^{-1} mol^{-1}	U_{POT}/kJ mol^{-1}	$\Delta U_{POT(-CH_2-)}$/kJ mol^{-1}	$\Delta U_{POT(-S-)}$/kJ mol^{-1}
[Taz(2,4)][Acgly]	519	38		424	8	
[Taz(2,4)][Acala]	557		29	416		5
[Taz(2,4)][Accys]	586			411		
^{b}[C_4mim][Gly]	426	39		447	10	
^{b}[C_4mim][Ala]	465			437		

^{a} Derived from previous work.[24] ^{b} Derived from ref. 38.

$$S^0 = 1246.5\ V_m + 29.5 \quad (5)$$

$$U_{POT} = 1981.2(\rho/M)^{1/3} + 103.8 \quad (6)$$

The S^0 and U_{POT} of ILs [Taz(2,4)][Acgly], [Taz(2,4)][Acala] and [Taz(2,4)][Accys] at 298.15 K are summarized in Table 4. The data reveal that the S^0 increases with the elongation of the anion side chain, indicating that longer side chains reduce structural order. Specifically, each additional –CH_2– group on the acetylated amino acid anion contributes 38 J K^{-1} mol^{-1} to the S^0, which aligns closely with the reported average contribution of 39 J K^{-1} mol^{-1} per –CH_2– group in [C_4mim][Gly] and [C_4mim][Ala].[19–21,38,39] Similarly, the incorporation of a sulfur atom into the anion side chain contributes 29 J K^{-1} mol^{-1} to the S^0.

Conversely, the U_{POT} decreases with the extension of the anion side chain. Each –CH_2– group added to the acetylated amino acid anion reduces the U_{POT} by 8 kJ mol^{-1}, consistent with the average contribution of −8 kJ mol^{-1} per –CH_2– group reported for 79 imidazolium-based ILs.[40] Additionally, the introduction of a sulfur atom into the anion decreases the U_{POT} by 5 kJ mol^{-1}. Compared to conventional inorganic salts, the significantly lower U_{POT} of ILs is the fundamental reason for their liquid state at room temperature.

3.3. The molar surface gibbs free energy and its applications

The relationship between the molar surface Gibbs energy, g_s, and temperature, T, is obtained by substituting eqn (7) into the traditional Eötvös equation,[31] which can be expressed as

$$g_S = V^{2/3}N^{1/3}\gamma \quad (7)$$

$$g_S = C_0 - C_1T \quad (8)$$

where V is molar volume, N is Avogadro constant and γ is surface tension. The values of g_s for [Taz(2,4)][Acgly], [Taz(2,4)][Acala] and [Taz(2,4)][Accys] are calculated, listed in Table 5 and plotted in Fig. 4. The predicted value of the molar surface Gibbs energy ($g_{s(pre)}$) can be calculated by the intercept C_0 and the slope C_1 into the eqn (8) and are shown in Table 5. According to thermodynamic relations, $C_1 = -(\partial g_s/\partial T)_p$ is the molar surface entropy (s) of ILs, and the molar surface enthalpy $h = g_s + sT$, and their values are listed in Table 5. The $g_{s(pre)}$ *versus* g_s of [Taz(2,4)][Acgly], [Taz(2,4)][Acala] and [Taz(2,4)][Accys] were

Table 5 Values of the molar surface Gibbs energy (g_s), molar surface entropy (s), molar surface enthalpy (h), predicted values of molar surface Gibbs energy ($g_{s(pre)}$), molar refraction (R_m), molar polarizability (α_p) and predicted values of surface tension (γ_{pre}) of [Taz(2,4)][Acgly], [Taz(2,4)][Acala] and [Taz(2,4)][Accys] in the range of T = (288.15–323.15) K

T/K	[a] ρ/kg m^{-3}	[a] 10^4V/m^3	g_s/kJ mol^{-1}	s/J mol^{-1} K^{-1}	h/kJ mol^{-1}	$g_{s(pre)}$/kJ mol^{-1}	γ_{pre}/mJ m^{-2}
[Taz(2,4)][Acgly]							
288.15	1150.61	2.350	14.93	17.12	19.66	14.93	45.9
293.15	1147.28	2.357	14.83	17.12	19.68	14.84	45.5
298.15	1143.95	2.364	14.75	17.12	19.70	14.75	45.2
303.15	1140.62	2.370	14.68	17.12	19.71	14.66	44.8
308.15	1137.29	2.377	14.58	17.12	19.70	14.56	44.5
313.15	1133.97	2.384	14.47	17.12	19.68	14.47	44.1
318.15	1130.66	2.391	14.36	17.12	19.66	14.38	43.8
323.15	1127.33	2.398	14.29	17.12	19.68	14.29	43.4
[Taz(2,4)][Acala]							
288.15	1122.90	2.533	15.69	19.30	21.25	15.70	46.4
293.15	1119.43	2.541	15.62	19.30	21.27	15.60	46.1
298.15	1115.96	2.549	15.51	19.30	21.27	15.51	45.7
303.15	1112.50	2.557	15.41	19.30	21.26	15.41	45.3
308.15	1109.03	2.564	15.30	19.30	21.25	15.31	44.9
313.15	1105.56	2.573	15.20	19.30	21.24	15.22	44.6
318.15	1102.08	2.581	15.13	19.30	21.27	15.12	44.2
323.15	1098.62	2.589	15.02	19.30	21.26	15.02	43.8
[Taz(2,4)][Accys]							
288.15	1184.92	2.671	16.36	19.26	21.91	16.38	46.8
293.15	1181.47	2.679	16.28	19.26	21.93	16.28	46.4
298.15	1178.04	2.687	16.21	19.26	21.95	16.19	46.0
303.15	1174.55	2.694	16.10	19.26	21.94	16.09	45.7
308.15	1171.04	2.703	15.99	19.26	21.93	15.99	45.3
313.15	1167.55	2.711	15.88	19.26	21.91	15.90	44.9
318.15	1164.07	2.719	15.81	19.26	21.93	15.80	44.6
323.15	1160.58	2.727	15.70	19.26	21.92	15.70	44.2

[a] Derived from previous work.[24]

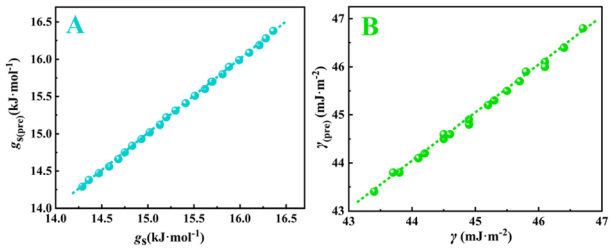

Fig. 4 Plot of (A) $g_{s(pre)}$ *vs.* g_s and (B) γ_{pre} *vs.* γ for [Taz(2,4)][Acgly], [Taz(2,4)][Acala] and [Taz(2,4)][Accys]. $g_{s(pre)} = 1.00021\ g_s - 0.00329$, $r^2 = 0.999$, sd = 0.0043; $\gamma_{(pre)} = 0.99767\ \gamma + 0.11354$, $r^2 = 0.998$, sd = 0.0116.

plotted in Fig. 4A. As can be seen, the h is independent with T, molar surface heat capacity is close to zero which indicates that the process from the inside to the surface of the liquid is an isocoulombic process.[41]

The equation for predicting the surface tension of ILs can be obtained using eqn (7) and (9):

$$\gamma_{pre}{}^{3/2} = [g_{s(pre)}{}^{3/2}/N^{1/2}R_m]n_D{}^2 - 1)/(n_D{}^2 + 2) \quad (9)$$

The predicted values of the surface tensions, γ_{pre}, for [Taz(2,4)][Acgly], [Taz(2,4)][Acala] and [Taz(2,4)][Accys] were also listed in Table 5. Fig. 4B shows the predicted surface tension γ_{pre} *versus* experimental surface tension γ of [Taz(2,4)][Acgly], [Taz(2,4)][Acala] and [Taz(2,4)][Accys]. As can be seen, the value of r^2 is equal to 0.99 suggesting that the proposed equation can well predict the ILs surface tension with low errors.

The association enthalpy of ion pairs in the gas phase ($\Delta_A H_m^0$) serves as a critical parameter for characterizing the strength of interionic interactions within liquid ionic liquids. Thermodynamically, when $\Delta_A H_m^0 < 0$, a larger absolute value indicates stronger ion association. The U_{POT}, vaporization enthalpy ($\Delta_g{}^1H_m^0$), and $\Delta_A H_m^0$ of ILs are interrelated through the following equation:[42]

$$\Delta_A H_m^0 = \Delta_g{}^1H_m^0 - U_{POT} \quad (10)$$

$$\Delta_g{}^1H_m^0 = 11.21\ (\gamma V^{2/3}N^{1/3}) + 2.4 \quad (11)$$

Here, $\Delta_g{}^1H_m^0$ is calculated *via* the Kabo empirical equation,[42] which depends on surface tension (γ), molar volume (V), and Avogadro's constant (N). The absolute values of $\Delta_A H_m^0$ for various ionic liquids are listed in Table 6.

Analysis of Table 6 reveals that introducing a methylene group or sulfur atom into the anion significantly reduces the absolute value of $\Delta_A H_m^0$ when the cation structure remains constant. This trend demonstrates that increasing the relative molecular mass of the anion weakens interionic associations within the ILs. Structural modification of anions, introducing methylene group or sulfur atom, significantly modulates the internal association strength of ILs through steric hindrance and charge delocalization effects. This principle provides a theoretical foundation for designing functionalized ILs with low melting points and high fluidity, particularly in applications requiring a balance between ionic conductivity and thermal stability.

3.4. Polarity

3.4.1. New scale of the polarity, δ_μ. In order to more accurately describe the polarity of ILs, Tong *et al.* proposed a new scale of the polarity, δ_μ, on the basis of three assumptions.[43] Based on Hildebrand's theory,[44] the solubility parameter of the polar part δ_μ is calculated:

$$\delta_\mu{}^2 = \Delta_g{}^1H_{m,\mu}^0/V - (1 - x)RT/V \quad (12)$$

where $x = \Delta_g{}^1H_{m,n}^0/\Delta_g{}^1H_m^0$, $\Delta_g{}^1H_m^0 = \Delta_g{}^1H_{m,n}^0 + \Delta_g{}^1H_{m,\mu}^0$ and the δ_μ is a new scale of the polarity. The vaporization enthalpy $\Delta_g{}^1H_m^0$ consists of non-polar part$\Delta_g{}^1H_{m,n}^0$ (the contribution part from the induced dipole moment to$\Delta_g{}^1H_m^0$) and polar part $\Delta_g{}^1H_{m,\mu}^0$ (the contribution part from the average permanent dipole moment to $\Delta_g{}^1H_m^0$). The values of $\Delta_g{}^1H_m^0$ and $\Delta_g{}^1H_{m,n}^0$ can be estimated by using Kabo empirical equation[45] and the Lawson–Ingham equation,[46] respectively.

$$\Delta_g{}^1H_{m,n}^0 = C[(n_D{}^2 - 1)/(n_D{}^2 + 2)]V \quad (13)$$

where $C = 1.297$ kJ cm^{-3} is an empirical constant for organic liquids, $n_D$is the refractive index and V is molar volume.

According to the eqn (10)–(13), the values of δ_μ, $\Delta_g{}^1H_m^0$, $\Delta_g{}^1H_{m,n}^0$ and $\Delta_g{}^1H_{m,\mu}^0$ for [Taz(2,4)][Acgly], [Taz(2,4)][Acala] and [Taz(2,4)][Accys] were calculated and listed in Table 7. It reveals the polarity order [Taz(2,4)][Acgly] > [Taz(2,4)][Acala] > [Taz(2,4)][Accys], demonstrating that the incorporation of methylene groups or sulfur atoms into the anion structure relatively enhances the hydrophobicity of ILs.

3.4.2. Improved new scale of the polarity, *P*. Unfortunately, the polarity of the solvent is the sum of all possible interactions between solvent and solute except chemical action, while the δ_μ only considers the dipole contribution part and does not

Table 6 Values of the surface tension (γ), molar volume (V), molar surface Gibbs free energy (g_s), molar vaporization enthalpy ($\Delta_g{}^1H_m^0$), lattice energy (U_{POT}) and association enthalpy of ion pairs ($\Delta_A H_m^0$) of [Taz(2,4)][Acgly], [Taz(2,4)][Acala] and [Taz(2,4)][Accys] at 298.15 K

ILs	γ/mJ m^{-2}	10^4 V/m^3 mol^{-1}	g_s/kJ mol^{-1}	$\Delta_g{}^1H_m^0$/kJ mol^{-1}	U_{POT}/kJ mol^{-1}	$\Delta_A H_m^0$/kJ mol^{-1}
[Taz(2,4)][Acgly]	45.2	2.363	14.75	167.7	424	−256.3
[Taz(2,4)][Acala]	45.7	2.549	15.51	176.3	416	−239.7
[Taz(2,4)][Accys]	46.1	2.687	16.21	184.1	411	−226.9

Table 7 The values of vaporization enthalpy ($\Delta_g{}^lH^0_m$), the contribution part from the induced dipole moment to vaporization enthalpy ($\Delta_g{}^lH^0_{m,n}$), the contribution part from the average permanent dipole moment to vaporization enthalpy ($\Delta_g{}^lH^0_{m,\mu}$), new scale of polarity (δ_μ) and polarity coefficient (P) for [Taz(2,4)][Acgly], [Taz(2,4][Acala] and [Taz(2,4][Accys] at $T = 298.15$ K

ILs	$\Delta_g{}^lH^0_m$/kJ mol^{-1}	$\Delta_g{}^lH^0_{m,n}$/kJ mol^{-1}	$\Delta_g{}^lH^0_{m,\mu}$/kJ mol^{-1}	$\delta\mu$/J$^{1/2}\cdot$cm$^{-3/2}$	P
[Taz(2,4)][Acgly]	167.7	89.15	78.60	18.10	0.939
[Taz(2,4)][Acala]	176.3	95.72	80.55	17.65	0.917
[Taz(2,4)][Accys]	184.1	105.37	78.75	17.00	0.865

consider the non-polar contribution part. Thus, Zhang *et al.*[27–29] took both dipole and non-polar contributions into account, modified δ_μ and deriving the equation for the polarity coefficient, P:

$$P = \delta_\mu/\delta_n = [(\Delta_g{}^lH^0_{m,\mu}/V - (1 - x)RT/V)/(\Delta_g{}^lH^0_{m,n}/V - xRT/V)]^{1/2} \quad (14)$$

In eqn (14), $(\Delta_g{}^lH^0_{m,\mu}/V) \gg [(1 - x)\ RT/V]$ and $(\Delta_g{}^lH^0_{m,n}/V) \gg (xRT/V)$. Thus, the following equation for calculating the polarity coefficient, P,

$$P = (\Delta_g{}^lH^0_{m,\mu}/\Delta_g{}^lH^0_{m,n})^{1/2} \quad (15)$$

P is called the polarity coefficient of ionic liquid, and the larger the value of polarity coefficient, the stronger the polarity of ILs (see Table 7).

From Table 7, the trends in P and δ_μ are identical, indicating that introducing methylene groups or sulfur atoms into the anion structure reduces the hydrophilicity of ILs, with sulfur atoms exhibiting a more pronounced effect. This is attributed to sulfur atoms significantly diminishing hydrophilicity through mechanisms such as charge delocalization, structural asymmetry, and dynamic hydrogen bond modulation-effects that surpass the steric hindrance-dominated contribution of methylene groups. Furthermore, the comparison between [C_4mim][BF_4] (P = 1.210) and [C_4mim][NTf_2] (P = 0.647) demonstrates that the polarity of [C_4mim][BF_4] is substantially higher than that of [C_4mim][NTf_2], consistent with empirical observations,[27] thereby confirming the broader applicability of P as a predictive metric for ILs polarity.

3.5. Viscosity

The temperature dependence of ILs viscosity can be correlated with various theoretical models. In addition to the VFT equation, the Arrhenius equation[47] is commonly employed to describe the temperature-dependent viscosity of ILs and calculate the viscous flow activation energy (E_η), which represents the minimum energy required for ion movement within the ILs. Another widely used equation relating viscosity to temperature is:

$$\ln \eta = \ln \eta_\infty - E_\eta/RT \quad (16)$$

where η_∞ is an empirical constant, E_η denotes the viscous flow activation energy, R represents the gas constant, and T is the absolute temperature. Using eqn (18), a linear fit of ln η *versus* T^{-1} was performed, with the fitting parameters and calculated results summarized in Table 8 and illustrated in Fig. 5. The E_η follow this order: [Taz(2,4)][Accys] (48.58 kJ mol^{-1}) < [Taz(2,4)][Acala] (51.18 kJ mol^{-1}) < [Taz(2,4)][Acgly] (64.68 kJ mol^{-1}).

Table 8 The values of activation Gibbs energy and activation energy for viscous flow of studied ILs

T/K	$^a\eta$/mPa s	E_η/kJ mol^{-1}	10^4V/m^{-3} mol^{-1}	$\Delta H^{\neq}$/kJ mol^{-1}	$\Delta G^{\neq}$/kJ mol^{-1}	$T\Delta S^{\neq}$/kJ mol^{-1}
[Taz(2,4)][Acgly]						
323.15	175.0	48.58	2.398	48.00	31.06	16.93
333.15	97.8	48.58	2.410	47.89	30.43	17.46
343.15	59.2	48.58	2.424	47.91	29.93	17.98
353.15	37.6	48.58	2.437	47.99	29.48	18.51
[Taz(2,4)][Acala]						
323.15	245.4	51.18	2.589	50.63	32.18	18.45
333.15	137.4	51.18	2.606	50.61	31.59	19.02
343.15	82.4	51.18	2.622	50.69	31.10	19.59
353.15	48.2	51.18	2.638	50.61	30.44	20.16
[Taz(2,4)][Accys]						
323.15	509.1	64.68	2.727	64.14	34.28	29.86
333.15	242.1	64.68	2.742	64.08	33.30	30.78
343.15	120.1	64.68	2.758	64.02	32.31	31.71
353.15	66.4	64.68	2.774	64.16	31.53	32.63

[a] Derived from previous work.[24]

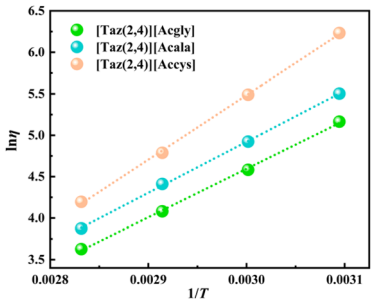

Fig. 5 Plot of ln η *vs.* 1/T for ILs [Taz(2,4)][Accys], [Taz(2,4)][Acala] and [Taz(2,4)][Acgly]. [Taz(2,4)][Acgly]: ln η = −12.94 + 5843.25/T, r^2 = 0.999, sd = 0.40962; [Taz(2,4)][Acala]: ln η = −13.54 + 6155.32/T, r^2 = 0.999, sd = 0.24198; [Taz(2,4)][Accys]: ln η = −17.86 + 7779.78/T, r^2 = 0.999, sd = 0.40962.

The E_η reflects the resistance to ion mobility and the energy barrier that ion pairs must overcome for mutual displacement. Higher activation energies indicate greater difficulty in ion pair separation, which may be attributed to factors such as larger ionic sizes, stronger intermolecular interactions, or more complex entanglement between ions in the ILs structure.[48] This observation aligns with previous reports correlating activation energy with the strength of cation–anion interactions and ionic liquid microstructural complexity.[28]

In studies of liquid transport properties, Eyring extended transition state theory to liquid flow phenomena, establishing a viscosity theory. According to the Eyring viscosity equation,[49] the relationship between viscosity and the activation Gibbs energy of viscous flow ($\Delta G^{\neq}$) is expressed as:

$$\eta = (hN/V)\exp(\Delta G^{\neq}/RT) \quad (17)$$

where η is viscosity, h is Planck's constant, N is Avogadro's number, V is molar volume, R is the gas constant, and T is temperature. Substituting experimental data into eqn (17), the calculated $\Delta G^{\neq}$ values for ILs at different temperatures are summarized in Table 8 and shown in Fig. 6. The descending order of $\Delta G^{\neq}$ magnitudes is: [Taz(2,4)][Accys] > [Taz(2,4)][Acala] > [Taz(2,4)][Acgly].

Using the thermodynamic relationship:

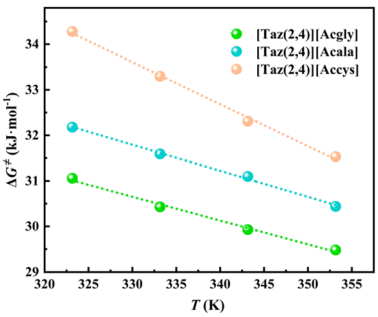

Fig. 6 Plot of $\Delta G^{\neq}$ *vs.* T for ILs [Taz(2,4)][Accys], [Taz(2,4)][Acala] and [Taz(2,4)][Acgly]. [Taz(2,4)][Acgly]: $\Delta G^{\neq}$ = 47.94−0.0524 T, r^2 = 0.991, sd = 0.00842; [Taz(2,4)][Acala]: $\Delta G^{\neq}$ = 50.64−0.0571 T, r^2 = 0.996, sd = 0.00487; [Taz(2,4)][Accys]: $\Delta G^{\neq}$ = 64.10−0.0924 T, r^2 = 0.996, sd = 0.01242.

$$\Delta G^{\neq} = \Delta H^{\neq} - \Delta S^{\neq} T \quad (18)$$

where $\Delta H^{\neq}$ and $\Delta S^{\neq}$ denote the activation enthalpy and entropy of viscous flow, respectively. Substituting eqn (18) into the Eyring viscosity equation and taking the natural logarithm yields:

$$\ln \eta = (R/\Delta S^{\neq}) \ln (hN/V) - \Delta H^{\neq}/RT \quad (19)$$

For moderate temperature ranges, $\Delta S^{\neq}$ can be considered constant. Notably, the E_η in the Arrhenius equation corresponds to $\Delta H^{\neq}$ in the Eyring framework. This equivalence arises because E_η represents the energy barrier for ion mobility, analogous to the enthalpy required to overcome intermolecular interactions during viscous flow.

As illustrated in Fig. 6, the $\Delta S^{\neq}$ for ILs is numerically equivalent to the slope of the linear fitting line. The calculated $T\Delta S^{\neq}$ values and $\Delta H^{\neq}$ derived from eqn (19) at various temperatures are compiled in Table 8. A comparison between $\Delta H^{\neq}$ values of the ILs [Taz(2,4)][Accys], [Taz(2,4)][Acala], and [Taz(2,4)][Acgly] and the Arrhenius E_η demonstrates close agreement between these two parameters. Crucially, eqn (19) enables a thermodynamic distinction between enthalpic ($\Delta H^{\neq}$) and entropic ($T\Delta S^{\neq}$) contributions to viscous flow resistance. Table 8 reveals that $\Delta H^{\neq} > T\Delta S^{\neq}$ for all ILs, indicating that the resistance to viscous flow is predominantly governed by enthalpic effects. This implies that ion mobility is primarily determined by the energy barrier $\Delta H^{\neq}$ required to overcome intermolecular interactions. Higher $\Delta H^{\neq}$ values correlate with stronger constraints on ion pair separation, reflecting increased difficulty for ions to move freely past one another. The dominance of enthalpic contributions aligns with the structural characteristics of ILs, where coulombic forces and hydrogen-bonding networks impose significant energy barriers to ion mobility.

4. Conclusions

This study developed and characterized three novel ILs [Taz(2,4)][Acgly], [Taz(2,4)][Acala] and [Taz(2,4)][Accys], investigating their physicochemical properties and structure–property relationships. Quantitative analysis of volumetric properties revealed that specific structural features of the anion systematically influence key molecular parameters. The introduction of each additional –CH_2– group resulted in a substantial increase in molecular volume (V_m), a significant elevation in standard molar entropy (S^0), and a noticeable reduction in lattice energy (U_{POT}). Furthermore, the incorporation of a sulfur atom also contributed to measurable increases in both V_m and S^0, while concurrently decreasing U_{POT}, albeit to a less pronounced extent compared to the –CH_2– group. Integration of molar surface Gibbs energ with the Lorentz–Lorenz equation yielded a predictive model for surface tension, demonstrating strong agreemen (r^2 = 0.99) between calculated and experimental values. Polarity characterization employed a new scale δ_μ, subsequently refined to the polarity coefficient P. Both metrics confirmed that anion modification *via* –CH_2– or –S– introduction reduces hydrophilicity, with sulfur imparting

a more significant hydrophobic enhancement. Viscosity analysis leveraged Eyring's equation and thermodynamic relations to derive activation enthalpy for viscous flow. These results corresponded closely with values from the Arrhenius equation, confirming enthalpic dominance in ion mobility resistance. Systematic modulation of IL properties through anion engineering enables predictive design for applications requiring tailored thermophysical behavior.

Author contributions

Conceptualization, D. F. and J. Q.; methodology, D. F. and L. L.; formal analysis, K. L. and J. M.; investigation, K. L. and H. Y.; resources, K. L. and J. Q.; data curation, K. L.; writing – original draft, K. L. and J. M.; writing – review and editing, K. L. and H. Y.; supervision, J. Q, and L. L.; funding acquisition, L. L., H. Y., and K. L. All authors have read and agreed to the published version of the manuscript.

Conflicts of interest

There are no conflicts to declare.

Data availability

The data supporting this article have been included as part of the supplementary information (SI), Supplementary information: 12 figures showing the ^{1}H NMR, ^{13}C NMR, IR, and TGA spectroscopy of the ILs [Taz(2,4)][Acgly], [Taz(2,4)][Acala] and [Taz(2,4)][Accys]. See DOI: **https://doi.org/10.1039/d5ra06386h**.

Acknowledgements

This work was supported by the National Natural Science Foundation of China (NSFC) (62201496), Special Funding of the Taishan Scholar Project (tsqn201909150), funding from the Qingchuang Science and Technology Plan of Shandong Universities (2023KJ283) and College Student Innovation and Entrepreneurship Training Program (S202310904130). Youth Entrepreneurship Talents Introduction Project in Shandong Province Higher Education Institutions.

Notes and references

1 C. Baudequin, D. Bregeon, J. G. F. Levillain, J. C. Plaquevent and A. C. Gaumont, Chiral ionic liquids, a renewal for the chemistry of chiral solvents? Design, synthesis and applications for chiral recognition and asymmetric synthesis, *Tetrahedron Asymmetry*, 2005, **16**, 3921–3945.

2 H. Clavier, L. Boulanger, N. Audi, L. Toupet, M. Mauduit and J. C. Guillemin, Design and synthesis of imidazolinium salts derived from (*L*)-valine. Investigation of their potential in chiral molecular recognition, *Chem. Commun.*, 2004, **10**, 1224–1225.

3 Y. Shimizu, Y. Ohte, Y. Yamamura, K. Saito and T. Atake, Low-temperature heat capacity of room-temperature ionic liquid, 1-hexyl-3-methylimidazolium bis(triflfluoromethylsulfonyl)imide, *J. Phys. Chem. B*, 2006, **110**, 13970–13975.

4 U. P. Yauheni, G. K. Andrey and V. B. Andrey, Calorimetric determination of the enthalpy of 1-butyl-3-methylimidazolium bromide synthesis: a key quantity in thermodynamics of ionic liquids, *J. Phys. Chem. B*, 2009, **113**, 14742–14746.

5 T. Brünig, K. Krekić, C. Bruhn and R. Pietschnig, Calorimetric Studies and Structural Aspects of Ionic Liquids in Designing Sorption Materials for Thermal Energy Storage, *Chem.–Eur. J.*, 2016, **22**, 16200–16212.

6 S. Chowdhury, R. S. Mohan and J. L. Scott, Reactivity of ionic liquids, *Tetrahedron*, 2007, **63**, 2363–2389.

7 K. Stappert, D. Unal, E. T. Spielberg and A. V. Mudring, Influence of the Counteranion on the Ability of 1-Dodecyl-3-methyltriazolium Ionic Liquids to Form Mesophases, *Cryst. Growth Des.*, 2015, **15**, 752–758.

8 K. Stappert and A. V. Mudring, Triazolium based ionic liquid crystals: Effect of asymmetric substitution, *RSC Adv.*, 2015, **5**, 16886–16896.

9 K. Stappert, D. Unal, B. Mallick and A. V. Mudring, New triazolium based ionic liquid crystals, *J. Mater. Chem. C*, 2014, **2**, 7976–7986.

10 Y. Jeong and J. S. Ryu, Synthesis of 1,3-dialkyl-1,2,3-triazolium ionic liquids and their applications to the Baylis- Hillman reaction, *J. Org. Chem.*, 2010, **75**, 4183–4191.

11 D. Chand, M. Wilk-Kozubek, V. Smetana and A. V. Mudring, Alternative to the Popular Imidazolium Ionic Liquids: 1,2,4-Triazolium Ionic Liquids with Enhanced Thermal and Chemical Stability, *ACS Sustainable Chem. Eng.*, 2019, **7**, 15995–16006.

12 S. Kirchhecker and D. Esposito, Amino acid based ionic liquids: A green and sustainable perspective, *Curr. Opin. Green Sustain. Chem.*, 2016, **2**, 28–33.

13 H. Ohno and K. Fukumoto, Amino Acid Ionic Liquids, *Acc. Chem. Res.*, 2007, **40**, 1122–1129.

14 K. Fukumoto, M. Yoshizawa and H. Ohno, Room Temperature Ionic Liquids from 20 Natural Amino Acids, *J. Am. Chem. Soc.*, 2005, **127**, 2398–2399.

15 O. J. Curnow and R. Yunis, Synthesis, characterization and properties of amino acid ionic liquids derived from the triaminocyclopropenium cation, *RSC Adv.*, 2016, **6**, 70152–70164.

16 M. P. Pereira, R. D. Souza Martins, M. A. L. De Oliveira and F. I. Bombonato, Amino acid ionic liquids as catalysts in a solvent-free Morita-Baylis-Hillman reaction Bombonato, *RSC Adv.*, 2018, **8**, 23903–23913.

17 S. Bhattacharyya and F. U. Shah, Thermal stability of choline based amino acid ionic liquids, *J. Mol. Liq.*, 2018, **266**, 597–602.

18 A. R. Jesusa, M. R. C. Soromenhoa, L. R. Raposob, J. M. S. S. Esperançaa, P. V. Baptistab, A. R. Fernandesb and P. M. Reisa, Enhancement of water solubility of poorly water-soluble drugs by new biocompatible N-acetyl amino acid N-alkyl cholinium-based ionic liquids, *Eur. J. Pharm. Biopharm.*, 2019, **137**, 227–232.

19 D. W. Fang, W. Guan, J. Tong, Z. W. Wang and J. Z. Yang, Study on physicochemical properties of ionic liquids based on alanine, *J. Phys. Chem. B*, 2008, **112**, 7499–7505.

20 D. W. Fang, J. Tong, W. Guan, H. Wang and J. Z. Yang, Predicting Properties of Amino Acid Ionic Liquid Homologue of 1-Alkyl-3-methylimidazolium Glycine, *J. Phys. Chem. B*, 2010, **114**, 13808–13814.
21 J. Z. Yang, Q. G. Zhang, B. Wang and J. Tong, Study on the Properties of Amino Acid Ionic Liquid EMIGly, *J. Phys. Chem. B*, 2006, **110**, 22521–22524.
22 Q. Yan, M. Liu, C. Y. Xiao, D. L. Fu, J. Wei, D. W. Fang and J. Z. Yang, Predicting properties of ionic liquid homologue of N-alkylpyridinium acetate, *J. Mol. Liq.*, 2021, **324**, 114720.
23 Q. Yan, J. Wei, J. Liu, Z. H. Zhang and D. W. Fang, Physicochemical properties of hydrophobic hexafluoroantimonate ionic liquids and applications of the mole surface Gibbs free energy, *Ionics*, 2020, **26**, 5585–5595.
24 K. H. Liang, Z. W. Lu, C. X. Ren, J. Wei and D. W. Fang, Feasibility of 1-Ethyl-4-butyl-1,2,4-triazolium Acetyl Amino Acid Ionic Liquids as Sustainable Heat-Transfer Fluids, *ACS Sustainable Chem. Eng.*, 2022, **10**, 3417–3429.
25 K. H. Liang, H. Y. Yao, J. Qiao, S. Gao, M. J. Zong, F. S. Liu, Q. L. Yang, L. J. Liang and D. w. Fang, Thermodynamic Evaluation of Novel 1,2,4-Triazolium Alanine Ionic Liquids as Sustainable Heat-Transfer Media, *Molecules*, 2024, **29**, 5227.
26 D. L. Fu, Z. R. Song, J. K. Liu, J. Yang, S. L. Suo, K. H. Liang, X. X. Ma and D. W. Fang, Low-temperature heat capacity and the thermodynamic functions of a novel ether-based ionic liquid 1-(2-ethoxyethyl)-3-ethylimidazolium thiocyanate, *RSC Adv.*, 2024, **14**, 34971.
27 D. Zhang, W. Jiang, L. Liu, K. Yu, M. Hong and J. Tong, The molar surface Gibbs energy and polarity of ether-functionalized ionic liquids, *J. Chem. Thermodyn.*, 2019, **138**, 313–320.
28 D. Zhang, B. Li, M. Hong, Y. X. Kong, J. Tong and W. G. Xu, Synthesis and characterization of physicochemical properties of new ether-functionalized amino acid ionic liquids, *J. Mol. Liq.*, 2020, **304**, 112718.
29 D. Zhang, Y. Qu, Y. Y. Gong, J. Tong, D. W. Fang and J. Tong, Physicochemical properties of [c$_n$mim][thr] (n= 3,5,6) amino acid ionic liquidss, *J. Chem. Thermodyn.*, 2017, **115**, 47–51.
30 H. F. D. Almeida, J. A. Lopes-da-Silva, M. G. Freire and J. A. P. Coutinho, Surface tension and refractive index of pure and water-saturated tetradecyltrihexylphosphonium-based ionic liquids, *J. Chem. Thermodyn.*, 2013, **57**, 372–379.
31 M. Deetlefs, K. R. Seddon and M. Shara, Predicting physical properties of ionic liquids, *Phys. Chem. Chem. Phys.*, 2006, **8**, 642–649.
32 B. W. Mountain and T. M. Seward, Hydrosulfide/sulfide complexes of copper(I): Experimental confirmation of the stoichiometry and stability of $Cu(HS)_2$-to elevated temperatures, *Geochim. Cosmochim. Acta*, 2003, **67**, 3005–3014.
33 C. L. Wei, K. Jiang, T. M. Fang and X. M. Liu, Effects of Anions and Alkyl Chain Length of Imidazolium-Based Ionic Liquids at the Au(111) Surface on Interfacial Structure: A First Principles Study, *Green Chem. Eng.*, 2021, **2**, 402–411.
34 A. Bhattacharjee, A. Luís, J. H. Santos, J. A. Lopes-da-Silva, M. G. Freire, P. J. Carvalho and J. A. P. Coutinho, Thermophysical properties of sulfonium- and ammonium-based ionic liquids, *Fluid Phase Equilib.*, 2014, **381**, 36–45.
35 Q. Wang, Z. G. Qu and D. Tian, Electric Double Layer Theory of Interfacial Ionic Liquids for Capturing Ion Hierarchical Aggregation and Anisotropic Dynamics, *Adv. Energy Mater.*, 2025, **15**, 2402974.
36 W. D. Tian, C. K. Zhang, S. Paul, W. D. Si, Z. Wang, P. P. Sun, A. Anoop, C. H. Tung and D. Sun, Lattice Modulation on Singlet-Triplet Splitting of Silver Cluster Boosting Near-Unity Photoluminescence Quantum Yield, *Angew. Chem., Int. Ed.*, 2025, **64**, e202421656.
37 S. Kang, Y. G. Chung, J. H. Kang and H. Song, CO_2 absorption characteristics of amino group functionalized imidazolium-based amino acid ionic liquids, *J. Mol. Liq.*, 2020, **297**, 111825.
38 J. Tong, M. Hong, Y. Chen, H. Wang, W. Guan and J. Z. Yang, The surface tension, density and refractive index of amino acid ionic liquids: [C_3mim][Gly] and [C_4mim][Gly], *J. Chem. Thermodyn.*, 2012, **54**, 352–357.
39 C. B. Zhou, J. Li, Z. Yi and H. J. Ai, Refractive Properties of Imidazolium Ionic Liquids with Alanine Anion [C$_n$mim][Ala] (n=2,3,4,5,6), *Russ. J. Phys. Chem. A*, 2017, **91**, 2044–2051.
40 D. Zhang, W. Jiang, L. Liu, K. Yu, M. Hong and J. Tong, The molar surface Gibbs energy and polarity of ether-functionalized ionic liquids, *J. Chem. Thermodyn.*, 2019, **138**, 313–320.
41 A. W. Adamson, *Physical Chemistry of Surfaces*, Wiley, New York, 1976, 3rd edn, 698.
42 Y. Meng, J. Liu, Z. Li and H. M. Wei, Synthesis and physicochemical properties of two SO_3H functionalized ionic liquids with hydrogen sulfate anion, *J. Chem. Eng. Data*, 2014, **59**, 2186–2195.
43 J. Tong, H. X. Yang, R. J. Liu, C. Li, L. X. Xia and J. Z. Yang, Determination of the Enthalpy of Vaporization and Prediction of Surface Tension for Ionic Liquid 1-Alkyl-3-methylimidazolium Propionate [C$_n$mim][Pro](n=4,5,6), *Phys. Chem. B*, 2014, **118**, 12972–12978.
44 J. H. Hildebrand and R. L. Scott, *The Solubility of Nonelectrolytes*, Reinhold, New York, 1950, 3rd edn.
45 A. A. Strechan, G. J. Kabo and Y. U. Paulechka, The correlations of the enthalpy of vaporization and the surface tension of molecular liquids, *Fluid Phase Equilib.*, 2006, **250**, 125–130.
46 D. D. Lawson and J. D. Ingham, Estimation of Solubility Parameters from Refractive Index Data, *Nature*, 1969, **223**, 614.
47 J. Vila, P. Ginés, J. M. Pico, C. Franjo, E. Jiménez, L. M. Varela and O. Cabeza, Temperature dependence of the electrical conductivity in EMIM-based ionic liquids-Evidence of Vogel-Tamman-Fulcher behavior, *Fluid Phase Equilib.*, 2006, **242**, 141–146.
48 M. Ebrahimi and F. Moosavi, The effects of temperature, alkyl chain length, and anion type on thermophysical properties of the imidazolium based amino acid ILs, *J. Mol. Liq.*, 2018, **250**, 121–130.
49 H. Eyring, Viscosity, plasticity, and diffusion as examples of absolute reaction rates, *J. Chem. Phys.*, 1936, **4**, 283–291.